Dynamic Modeling of an L-Shape PMN-PT Piezo-Based Manipulator

Jingang Yi, Steven Chang, Kee Moon, and Yang Shi

Abstract— In this paper, we present a modeling scheme of a cantilever-based L-shape manipulator. The L-shape manipulator is made of $(1-x)\mathbf{Pb(Mg_{1/3}Nb_{2/3})O_3}$-$x\mathbf{PbTiO_3}$ (PMN-PT) single-crystal relaxor ferroelectric material. We first report the design of a novel cantilever capable of motion in multiple degrees of freedom. The top and bottom surfaces of the L-shape cantilever structure are printed with interdigitated electrode (IDE), which allow the structure to produce both axial and flexural independently. The dynamic modeling of such a manipulation structure are discussed and presented. The analytical modeling results match well with the finite element analysis and experimental results. The controlled planar manipulator has potential applications in micro- and nano-applications, such as nano-indentation.

I. INTRODUCTION

During the last decade, micro-/nano-manipulation have been extensively studied in robotics and control communities. For example, the atomic force microscope (AFM) has been considered one of the platforms to carry out manipulation and assembly at micro- or nano-scale [1]–[4]. A good review of robotic micro- and nano-manipulation can be found in [5] and [6].

For manipulation platforms, for example, AFMs, piezoelectric cantilever beams are the most widely used actuation mechanisms. Piezoelectric film actuators such as bimorphs and unimorphs are one of the most widely employed forms of smart material actuators because of their simple design and large bending deflection. In the case of a bimorph, one piezo-film elongates while the other contracts, and produces a flexural motion. In general, stack-type actuators are used to obtain a linear (axial) motion. The actuator consists of a stack of piezoelectric disks and exhibits a high stiffness motion. The displacement generated by this type of actuator has the same direction as the direction of polarization electric field.

A single-crystal relaxor ferroelectric material, such as PMN-PT $(1-x)\mathrm{Pb(Mg_{1/3}Nb_{2/3})O_3}$-$x\mathrm{PbTiO_3}$, is a potential candidate for new generation actuator and sensor applications due to their high piezoelectric coefficients [7]. New PMN-PT piezo-devices have been developed in recent years. For example, Hong *et al.* [8] develop a PMN-PT-based smart cantilever structure that is capable of both sensing and actuation. In [9], interdigitated electrodes (IDE) have been employed to utilize the high piezoelectric coupling along d_{33} direction. It is demonstrated that a PMN-PT unimorph with IDE design can generate both a longitudinal and flexural motion without any additional passive or active layers [10]. Both the axial and flexural motions are produced by differentially controlling the contraction/elongation of the top and bottom IDEs of the cantilever.

In [11], a PMN-PT unimorph L-shape structure is designed and fabricated as a multi-degree-of-freedom (MDOF) manipulator. The L-shaped manipulator combines two PMN-PT-based cantilevers to form one monolithic structure (Fig. 1(c)). The manipulator has a set of four independent IDEs on the top and bottom surfaces of each cantilever. Therefore, the manipulator is capable of motion in four degrees of freedom. The manipulator design has several advantages over the conventional cantilever design for micro-/nano-manipulation. The L-shape manipulator provides motion in multiple degrees of freedom at the end effector and therefore enables more complicated manipulation, such as twisting. Most cantilever-based manipulators, such as those used in AFM, can only provide flexural motion. Additionally, the proposed MDOF manipulator is very compact and portable.

The goal of this paper is to develop a mathematical model for the L-shape manipulator. Several reasons motivate us to develop such an analytical model. First, we need to understand the dynamic properties and characteristics of the manipulation device. Second, we need a mathematical model of the manipulator to design advanced control systems. Since the manipulator provides motion in multiple degrees of freedom, a model-based control system is necessary to guide the manipulation and assembly actions. In [12], [13], dynamic analysis of an L-shape frame is studied. Although the frame motion in [14] is in three-dimensional space, the results in [14] cannot be applied to our manipulator because we need to consider both the axial and flexural motions produced by the L-shape structure.

The remainder of the paper is organized as follows. In Section II, we describe the PMN-PT-based manipulator design. The dynamic models of the L-shape manipulator are presented in Section III. Then we demonstrate the validity of the models through a comparison with numerical and experimental results in Section IV. We conclude the paper in Section V.

II. PMN-PT MANIPULATOR DESIGN

In this section, we first describe the basic principles for the PMN-PT cantilever beam actuators and then discuss the L-shape manipulator design.

Fig. 1(b) shows a schematic diagram of a PMN-PT cantilever beam. The IDE electrodes are identical on the top and

J. Yi, S. Chang, K. Moon are with the Department of Mechanical Engineering, San Diego State University, San Diego, CA 92182, USA. Email: {jgyi,kmoon}@mail.sdsu.edu (J. Yi and K. Moon), and changs@rohan.sdsu.edu (S. Chang).

Y. Shi is with the Department of Mechanical Engineering, University of Saskatchewan, Saskatoon, Saskatchewan Canada S7N 5A9. Email:yang.shi@usask.ca.

the bottom of a PMN-PT cantilever. A pair of electrode fingers with positive and negative electrode potentials induces an electric field with a dominant axial component that is parallel to the poling direction (along the x-axis direction, that is, high piezoelectric constant d_{33} along the 33 direction shown in Fig. 1(b)). The PMN-PT cantilever in combination with the IDE design can generate two motions, one in the axial direction and the other in the flexural direction.

The distribution of electric field is built up strongly between two IDE fingers on both the top and bottom of the actuator surfaces. The dominant axial (longitudinal) piezoelectric component (e.g. high d_{33} values) of the PMN-PT material causes a primarily axial piezoelectric deformation. The active fields are responsible for the overall axial deformation. Fig. 2(a) shows that a 9 V (peak-to-peak) sinusoidal input voltage (1 Hz) at both IDE electrodes yields about a 0.25-μm (peak-to-peak) axial displacement [11]. The dimension of the PMN-PT cantilever actuator is roughly about 10 mm $\times$ 1.5 mm $\times$ 110 μm. The prototype of the cantilever is shown in Fig. 1(a) and is designed and fabricated using the SDSU and UCI micro-fabrication facilities.
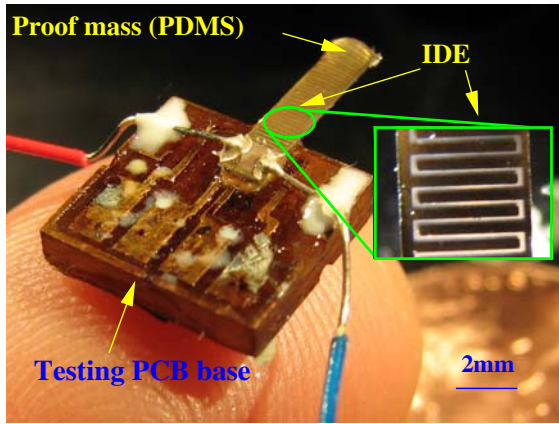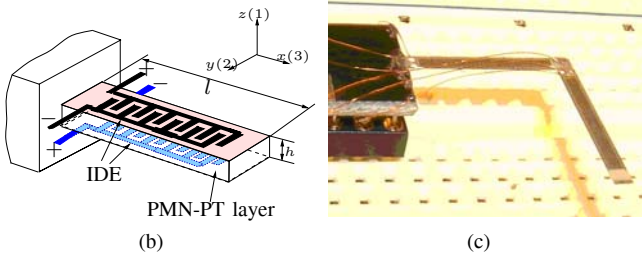
Fig. 1. (a) A PMN-PT/PDMS cantilever prototype. (b) A schematic of a single PMN-PT cantilever beam. (c) L-shape manipulator prototype made of two cantilevers.

Moreover, the PMN-PT film actuator can also provide a flexural displacement by activating both sides of the cantilever in opposite directions. The working principle is similar to that of a piezoelectric bimorph with two imaginary active layers. The top and bottom IDEs are operated in opposite modes (contraction/expansion). The resulting effect will cause the film to bend and thus produce a flexural motion. Fig. 2(b) shows that a 2 V (peak-to-peak) 1 Hz input voltage signal at both IDE electrodes yields about a 2-μm

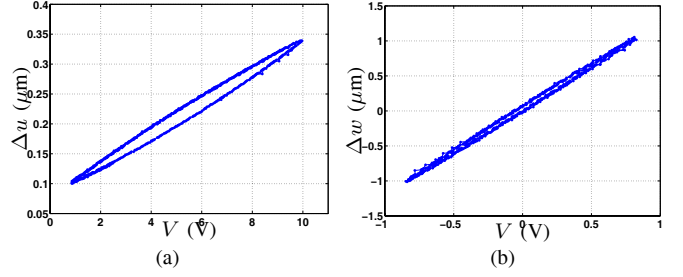flexural displacement with a small-amplitude hysteresis [11].

Fig. 2. (a) Axial deflection under a sinusoidal input voltage. (b) Flexural deflection under a sinusoidal input voltage.

The L-shape composite structure shown in Fig. 1(c) consists of two cantilever beams. Due to the simple fabrication of a PMN-PT cantilever beam, we use two PMN-PT cantilever beams to form the L-shape structure. The connection between these two cantilevers can be considered as rigid.

Since the L-shape structure is made of two separate cantilever beams, we control each cantilever beam using their respective top and bottom IDEs and therefore manipulate the motion of the structure. In the following, we first discuss the dynamics of the single cantilever beam and then extend to the L-shape structure.

III. DYNAMIC MODELING

A. Single cantilever structure

For the single cantilever PMN-PT structure, we consider the both axial and flexural vibrational motion. We denote the size of the PMN-PT cantilever beam as l (length) $\times$ b (width) $\times$ h (height). We set up the coordinate system such that the x-axis is along the axial direction and the deflection is within xz-plane. For the fixed inertial frame $\mathcal{F}_a$, the unit vector along x, y, and z-axes are $\mathbf{a}_1$, $\mathbf{a}_2$, and $\mathbf{a}_3$, respectively; see Fig. 4. We denote the axial displacement and flexural deflection as $u(x,t)$ and $w(x,t)$, respectively. We obtain the position vector $\mathbf{r}(x,t)$ as

$$
\begin{aligned}
\mathbf{r}(x,t) &= \left(u(x,t) - z\frac{\partial w}{\partial x} \right) \mathbf{a}_1 + w(x,t)\mathbf{a}_3 \\
&\approx u(x,t)\mathbf{a}_1 + w(x,t)\mathbf{a}_3.
\end{aligned} \tag{1}
$$

Because deflections are small, we can drop the term $z\frac{\partial w}{\partial x}$ in the above equation. Then the velocity is obtained as

$$
\mathbf{v}(x,t) = \dot{u}(x,t)\mathbf{a}_1 + \dot{w}(x,t)\mathbf{a}_3. \tag{2}
$$

We consider the kinetic energy of the system

$$
T = \frac{1}{2}\int_0^l m\mathbf{v}\cdot\mathbf{v}\,dx, \tag{3}
$$

where m is the mass density per unit length. For potential energy U, we obtain

$$
U = \frac{1}{2}\int_0^l \left[EI\left(\frac{\partial^2 w}{\partial x^2}\right)^2 + EA\left(\frac{\partial u}{\partial x}\right)^2 \right] dx, \tag{4}
$$

where E is the Young's modulus, I and A are the second moment of area of the cross-section of the beam, respectively.

We consider the forces and moments generated by the input voltage through IDEs. Let V_T and V_B be the voltages applied on the top and bottom IDEs, respectively. Fig. 3(a) shows the IDE-generated electric fields inside PMN-PT and Fig. 3(b) shows the schematic of the distribution of axial strains due to the electric field in the xz plane across the center of the cantilever beam. We denote the distance between IDE fingers as h_F. The strains generated by V_T and V_B at the top and bottom surfaces of PMN-PT cantilever are

$$\epsilon_T(x,t) = \frac{V_T(x,t)d_{33}}{h_F}, \quad \epsilon_B(x,t) = \frac{V_B(x,t)d_{33}}{h_F}, \quad (5)$$

where d_{33} is the piezoelectric constant along the 33 direction. Since the IDEs are assumed to be perfect on the PMN-PT surfaces, we assume that the strain distribution is continuous along the xz cross-section (see Fig. 3(b)). We denote the vertical distance between the bottom surface and the neutral axis as D. Then we have

$$\frac{D}{D+h} = \frac{\epsilon_B}{\epsilon_T} = \frac{V_B}{V_T}, \quad (6)$$

thus for $V_T \neq V_B$, $D = \frac{V_B}{V_T - V_B}h$, where we drop the variable dependencies on x and t for brevity. We can calculate the resultant axial force F_n and moment M_n around the beam central line NN' (Fig. 3(b)) due to the strain distribution generated by the input voltages on both IDEs.
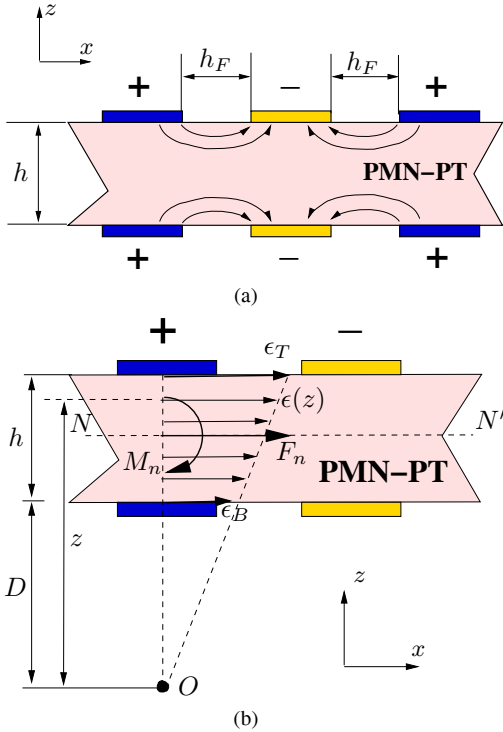

(a)

(b)

Fig. 3. (a) Electric field distribution inside PMN-PT around IDEs and (b) axial strain distributions due to applied voltages.

Considering the strain distribution in Fig. 3(b) and using Eqs. (5) and (6), we obtain the strain at location z as

$$\epsilon(z) = \frac{z}{D+h}\epsilon_T = \frac{z(V_T - V_B)d_{33}}{hh_F}.$$

Thus, we obtain the resultant axial force $F_n(x,t)$

$$F_n(x,t) = \int_D^{D+h} \sigma(z)b\,dz = \frac{Ebd_{33}h}{2h_F}(V_T + V_B), (7)$$

where $\sigma(z) = E\epsilon(z)$ is the axial stress at location z. Similarly, the resultant moment M_n around the center line NN' is

$$M_n(x,t) = -\frac{Ebd_{33}h^2}{12h_F}(V_T - V_B). \quad (8)$$

The virtual work done by the axial force and moment is

$$\delta W_{nc} = \int_0^l \left(F_n'(x,t)\delta u + M_n''(x,t)\delta w \right) dx. \quad (9)$$

Using the extended Hamilton's principles [15] and Eqs. (3), (4) and (9), we obtain the equations of the motion as

$$m\frac{\partial^2 u}{\partial t^2} - EA\frac{\partial^2 u}{\partial x^2} = F_n'(x,t), \quad (10a)$$

$$m\frac{\partial^2 w}{\partial t^2} + EI\frac{\partial^4 w}{\partial x^4} = M_n''(x,t), \quad (10b)$$

and boundary conditions

$$u(0,t) = 0, \ w(0,t) = 0, \ w'(0,t) = 0, \ u'(l,t) = 0, \quad (11a)$$

$$EIw^{(2)}(l,t) = 0, \quad EIw^{(3)}(l,t) = 0, \quad (11b)$$

where we use the notation $\dot{f}(x,t) = \frac{\partial f}{\partial t}$ and $f^{(n)}(x,t) = \frac{\partial^n f}{\partial x^n}$ for a function $f(x,t)$.

Note that dynamics of the axial and flexural directions are decoupled from each other. Therefore, we can calculate the natural frequencies for axial and flexural motion separately. For axial and flexural motions with the above boundary conditions, we obtain their respective natural frequencies as [15]

$$\omega_k^a = \frac{(2k-1)\pi}{2}\sqrt{\frac{EA}{mL^2}}, \ \omega_k^f = c_k\sqrt{\frac{EI}{mL^4}}, \quad k = 1, 2, \cdots,$$

where $c_1 = 1.875$, $c_2 = 4.694$, $c_3 = 7.855$, etc.

Comparing ω_k^a and ω_k^f for the rectangular cross-section cantilever beam with the thickness much less than the width and length, we find that $\omega_k^f \ll \omega_k^a$. Therefore, the natural frequencies of the beam follows closely with the flexural motion for the first few modes.

B. L-shape cantilever structure

Fig. 4 shows the motion schematic of the L-shape manipulator. Here we assume that the motion of the manipulator is small compared with its size. We consider an L-shape structure that consists of two cantilever with length l_1 and l_2, respectively. We assume that the orientation angle between the two beams is 90 degrees, namely, they are perpendicular to each other. Each beam can move independently along the axial and flexural directions. We set up the coordinate systems as shown in Fig. 4. For the body-fixed moving frame $\mathcal{F}_b$ along beam #2, the unit vectors along x_2, y_2, and z_2-axes are $\mathbf{b}_1$, $\mathbf{b}_2$, and $\mathbf{b}_3$, respectively. For simplicity, we assume that beam #1 only vibrates or moves in the x_1z_1 plane and
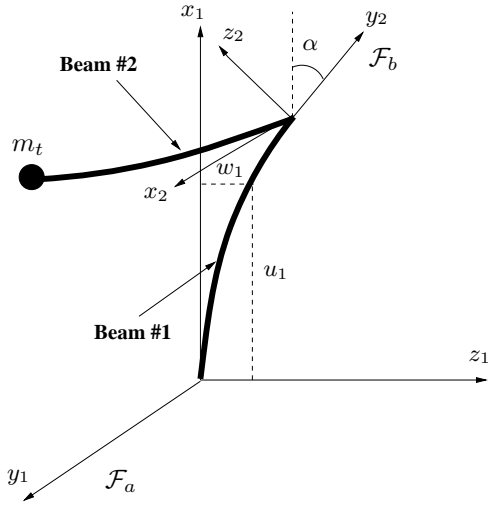
Fig. 4. A kinematics schematic of the L-shape manipulator.

beam #2 only in the x_2-z_2 plane. We also consider a point mass m_t that is attached at the tip of beam #2.

We denote the displacements of beam #i along the x_i and z_i axes as u_i and w_i, $i = 1, 2$, respectively. We also denote the deflection angle of the tip of beam #1 as α (Fig. 1(c)), namely, $\alpha = \left.\frac{\partial w_1}{\partial x_1}\right|_{x_1 = l_1}$. Then the coordinate transformation matrix C_{ba} from frames $\mathcal{F}_b$ to the fixed frame $\mathcal{F}_a$ can be obtained as

$$C_{ba} = \begin{bmatrix} 0 & 1 & 0 \\ \cos\alpha & 0 & \sin\alpha \\ \sin\alpha & 0 & -\cos\alpha \end{bmatrix}. \qquad (12)$$

Assuming small deflections for both beams, we write the position vectors $\mathbf{r}_1$ and $\mathbf{r}_2$ of the differential elements on beams #1 and #2, respectively, as

$$\mathbf{r}_1 \approx u_1(x_1, t)\mathbf{a}_1 + w_1(x_1, t)\mathbf{a}_3 \qquad (13)$$

and

$$\mathbf{r}_2 \approx u_1(l_1, t)\mathbf{a}_1 + w_1(l_1, t)\mathbf{a}_3 \\ + u_2(x_2, t)\mathbf{b}_1 + w_2(x_2, t)\mathbf{b}_3. \qquad (14)$$

We drop the terms $z_i \frac{\partial w_i}{\partial x_i}$ in the above equations due to $\alpha \ll 1$. Using the transformation matrix C_{ba}, we can write Eq. (14) into frame $\mathcal{F}_a$ as

$$\mathbf{r}_2 = [\mathbf{r}_1(l_1, t) + w_2(x_2, t)\sin\alpha]\mathbf{a}_1 + u_2(x_2, t)\mathbf{a}_2 + \\ [w_1(l_1, t) - w_2(x_2, t)\cos\alpha]\mathbf{a}_3. \qquad (15)$$

For velocities, we obtain

$$\mathbf{v}_1(x_1, t) = \dot{u}_1(x_1, t)\mathbf{a}_1 + \dot{w}_1(x_1, t)\mathbf{a}_3, \qquad (16)$$
$$\mathbf{v}_2(x_2, t) = \dot{\mathbf{r}}_2 \approx \dot{u}_1(l_1, t)\mathbf{a}_1 + \dot{u}_2(x_2, t)\mathbf{a}_2 + \\ [\dot{w}_1(l_1, t) - \dot{w}(x_2, t)]\mathbf{a}_3. \qquad (17)$$

In Eq. (17), we drop the nonlinear terms (e.g. $\alpha\dot{w}_2$) again due to a small α.

We consider the kinetic energy of the system

$$T = T_1 + T_2 + T_t, \qquad (18)$$

where $T_i = \frac{1}{2}\int_0^{l_i} m_i\mathbf{v}_i \cdot \mathbf{v}_i dx_i$, $i = 1, 2$, and $T_t = \frac{1}{2}m_t\mathbf{v}_2(l_2, t) \cdot \mathbf{v}_2(l_2, t)$. In the above equations, m_i is the mass per unit length for beam #i. For potential energy V, we obtain

$$V = \frac{1}{2}\sum_{i=1}^2 \int_0^{l_i} \left[E_i I_i \left(\frac{\partial^2 w_i}{\partial x_i^2}\right)^2 + E_i A_i \left(\frac{\partial u_i}{\partial x_i}\right)^2 \right] dx_i,$$

where E_i is the Young's modulus, I_i and A_i are the second area moment of inertia and area for the cross-section of beam #i, respectively. For the non-conservative work done by the forces and moments due to the input controlled voltage through the IDEs, we follow a similar calculation to that of the single cantilever beam case and obtain

$$\delta W_{nc} = \sum_{i=1}^2 \int_0^{l_i} (F'_{ni}(x_i, t)\delta u_i + M''_{ni}(x_i, t)\delta w_i) \, dx_i,$$

where $F_{ni}(x_i, t)$ and $M_{ni}(x_i, t)$ are the resultants force and moments for the ith beam at location x_i and time t, respectively.

Using the extended Hamilton's principles, we can derive the dynamic equations for the manipulator as follows.

$$m_1\frac{\partial^2 u_1}{\partial t^2} - E_1 A_1\frac{\partial^2 u_1}{\partial x_1^2} = F'_{n1}, \qquad (19a)$$

$$m_1\frac{\partial^2 w_1}{\partial t^2} + E_1 I_1\frac{\partial^4 w_1}{\partial x_1^4} = M''_{n1}, \qquad (19b)$$

$$m_2\frac{\partial^2 u_2}{\partial t^2} - E_2 A_2\frac{\partial^2 u_2}{\partial x_2^2} = F'_{n2}, \qquad (19c)$$

$$m_2\left[\ddot{w}_1(l_1, t) - \frac{\partial^2 w_2}{\partial t^2}\right] - E_2 I_2\frac{\partial^4 w_2}{\partial x_2^4} = M''_{n2} \qquad (19d)$$

and boundary conditions

$$u_1(0, t) = 0, \quad w_1(0, t) = 0, \quad u'_1(0, t) = 0,$$
$$w'_1(0, t) = 0, \quad u_2(0, t) = 0, \quad w_2(0, t) = 0, \qquad (20a)$$
$$u'_2(0, t) = 0, \quad w'_2(0, t) = 0, \quad w''_1(l_1, t) = 0,$$
$$w''_2(l_2, t) = 0, \qquad (20b)$$

$$\int_0^{l_2} m_2\ddot{u}_1(l_1, t)dx_2 + m_t\ddot{u}_1(l_1, t) + E_1 A_1 u'_1(l_1, t) = 0, \qquad (20c)$$

$$\int_0^{l_2} m_2[\ddot{w}_1(l_1, t) - \ddot{w}_2] dx_2 + m_t[\ddot{w}_1(l_1, t) - \ddot{w}_2(l_2, t)]$$
$$- E_1 I_1 w_1^{(3)}(l_1, t) = 0, \qquad (20d)$$
$$m_t\ddot{u}_2(l_2, t) + E_2 A_2 u'_2(l_2, t) = 0, \qquad (20e)$$
$$m_t[\ddot{w}_1(l_1, t) - \ddot{w}_2(l_2, t)] + E_2 I_2 w_2^{(3)}(l_2, t) = 0. \qquad (20f)$$

To compute the natural frequencies of the L-shape structure, we first define the following non-dimensional variables [14].

$$\zeta_i = \frac{x_i}{l_i}, \; M = \frac{m_2}{m_1}, \; M_t = \frac{m_t}{m_1 l_1}, \; L = \frac{l_2}{l_1},$$
$$\lambda_{ui}^2 = \frac{m_i l_i^2 \omega^2}{E_i A_i}, \; \lambda_{wi}^4 = \frac{m_i l_i^4 \omega^2}{E_i I_i}, \quad i = 1, 2. \qquad (21)$$

Assuming a separable solution $u_i(x_i, t) = l_i U_i(\zeta_i) e^{j\omega t}$, $w_i(x_i, t) = l_i W_i(\zeta_i) e^{j\omega t}$, $i = 1, 2$, then Eqs. (19) become

$$U_i'' + \lambda_{ui}^2 U_i = 0, \tag{22a}$$

$$W_1^{(4)} - \lambda_{w1}^4 W_1 = 0, \tag{22b}$$

$$W_2^{(4)} - \lambda_{w2}^4 \left(W_2 - \frac{1}{L} W_1(1) \right) = 0. \tag{22c}$$

And boundary conditions (20) become

$$U_1(0) = 0, \ W_1(0) = 0, \ W_1'(0) = 0,$$
$$W_2'(0) = 0, \ U_2(0) = 0, \tag{23a}$$
$$W_2(0) = 0, \ U_1'(0) = 0, \ U_2'(0) = 0,$$

$$W_1''(1) = 0, \ W_2''(1) = 0, \tag{23b}$$

$$U_1' - \lambda_{u1}^2 (ML + M_t) U_1(1) = 0, \tag{23c}$$

$$\int_0^1 ML \lambda_{w1}^4 [W_1(1) - LW_2(\zeta_2)] \, d\zeta_2 +$$
$$\lambda_{w1}^4 M_t [W_1(1) - LW_2(1)] + W_1^{(3)}(1) = 0, \tag{23d}$$

$$U_2'(1) - \frac{M_t}{ML} U_2(1) = 0, \tag{23e}$$

$$\lambda_{w2}^4 \frac{M_t}{ML^2} [W_1(1) - LW_2(1)] - W_2^{(3)}(1) = 0. \tag{23f}$$

Since the motion equations in the axial and flexural directions are decoupled, we consider one direction at a time and then compare the calculated natural frequencies etc. like in the single cantilever beam case. The general solutions for (22b) and (22c) are, respectively,

$$W_1(\zeta_1) = B_1 \sin(\lambda_{w1}\zeta_1) + B_2 \cos(\lambda_{w1}\zeta_1) +$$
$$B_3 \sinh(\lambda_{w1}\zeta_1) + B_4 \cosh(\lambda_{w1}\zeta_1),$$
$$W_2(\zeta_2) = C_1 \sin(\lambda_{w2}\zeta_2) + C_2 \cos(\lambda_{w2}\zeta_2) +$$
$$C_3 \sinh(\lambda_{w2}\zeta_2) + C_4 \cosh(\lambda_{w2}\zeta_2) + \frac{1}{L} W_1(1),$$

where B_i and C_i, $i = 1, 2, 3, 4$, are coefficients to be determined by the boundary conditions. We define the coefficient vector $\mathbf{q} = [B_1 \ B_2 \ C_1 \ C_2 \ C_4]^T \in \mathbb{R}^5$. Using boundary conditions (23b), (23c), (23d), and (23f), we obtain the following matrix equations for $\mathbf{q}$.

$$\mathcal{A}\,\mathbf{q} = \mathbf{0}, \tag{24}$$

where $\mathcal{A} \in \mathbb{R}^{5\times5}$ is given as

$$\mathcal{A} = \begin{bmatrix} A_{11} & A_{12} & 0 & 0 & 0 \\ A_{21} & A_{22} & 0 & L & L \\ 0 & 0 & s_{\lambda_{w2}} + sh_{\lambda_{w2}} & c_{\lambda_{w2}} & -ch_{\lambda_{w2}} \\ A_{41} & A_{42} & A_{43} & A_{44} & A_{45} \\ 0 & 0 & A_{53} & A_{54} & A_{55} \end{bmatrix}, \tag{25}$$

where we denote $s_{\lambda_{wi}} = \sin(\lambda_{wi})$, $c_{\lambda_{wi}} = \cos(\lambda_{wi})$,

$sh_{\lambda_{wi}} = \sinh(\lambda_{wi})$, $ch_{\lambda_{wi}} = \cosh(\lambda_{wi})$, $i = 1, 2$, and

$$A_{11} = s_{\lambda_{w1}} + sh_{\lambda_{w1}}, \ A_{12} = c_{\lambda_{w1}} + ch_{\lambda_{w1}},$$
$$A_{21} = s_{\lambda_{w1}} - sh_{\lambda_{w1}}, \ A_{22} = c_{\lambda_{w1}} - ch_{\lambda_{w1}},$$
$$A_{41} = c_{\lambda_{w1}} + ch_{\lambda_{w1}}, \quad A_{42} = -(s_{\lambda_{w1}} - sh_{\lambda_{w1}}),$$
$$A_{43} = \frac{ML^2 \lambda_{w1}}{\lambda_{w2}} (2 - c_{\lambda_{w2}} - ch_{\lambda_{w2}}) + \lambda_{w1} M_t (s_{\lambda_{w2}} -$$
$$sh_{\lambda_{w2}}), \quad A_{44} = ML^2 \frac{\lambda_{w1}}{\lambda_{w2}} s_{\lambda_{w2}} + \lambda_{w1} M_t c_{\lambda_{w2}},$$
$$A_{45} = ML^2 \frac{\lambda_{w1}}{\lambda_{w2}} sh_{\lambda_{w2}} + \lambda_{w1} M_t ch_{\lambda_{w2}},$$
$$A_{53} = \left[-(c_{\lambda_{w2}} + ch_{\lambda_{w2}}) + \frac{\lambda_{w2} M_t}{ML} (s_{\lambda_{w2}} - sh_{\lambda_{w2}}) \right],$$
$$A_{54} = s_{\lambda_{w2}} + \frac{\lambda_{w2} M_t}{ML} c_{\lambda_{w2}}, \ A_{55} = sh_{\lambda_{w2}} + \frac{\lambda_{w2} M_t}{ML} ch_{\lambda_{w2}}.$$

To have non-trivial solutions, we have $\det \mathcal{A} = 0$ and the natural frequencies need to satisfy

$$-2ML^2 \lambda_{w2} \mathbf{F_{cf1}} \mathbf{F_{cf2}} + 2M_t L \lambda_{w2}^2 \mathbf{F_{cf1}} \mathbf{F_{cs1}} +$$
$$2M_t \lambda_{w1} \lambda_{w2}^2 (M - M_t)(s_{w2} - sh_{w2}) c_{w2} ch_{w2} \mathbf{F_{cs1}} +$$
$$2M^2 L^3 \lambda_{w1} \mathbf{F_{cs1}} \mathbf{F_{cr2}} + ML \lambda_{w1} \lambda_{w2} (M + M_t)$$
$$(c_{w2} + ch_{w2}) \mathbf{F_{cs1}} + 2MM_t L^2 \lambda_{w1} \lambda_{w2} [2c_{w2} ch_{w2} -$$
$$(c_{w2} + ch_{w2})] \mathbf{F_{cs1}} + ML \lambda_{w1} \lambda_{w2} (M - M_t) [(c_{w2} -$$
$$ch_{w2}) s_{w2} sh_{w2} - (c_{w2} + ch_{w2}) c_{w2} ch_{w2}] \mathbf{F_{cs1}} = 0, \quad (26)$$

where

$$\mathbf{F_{cf}}_i = 1 + c_{wi} ch_{wi}, \ \mathbf{F_{cs}}_i = s_{wi} ch_{wi} - c_{wi} sh_{wi},$$
$$\mathbf{F_{cr}}_i = s_{wi} ch_{wi} + c_{wi} sh_{wi}. \tag{27}$$

In the single beam natural frequencies equations given in (27), the subscripts "$\mathbf{c}$", "$\mathbf{f}$", "$\mathbf{s}$", and "$\mathbf{r}$" represent clamped, free, supported, and roller ends [13], respectively.

IV. EXPERIMENTAL RESULTS

We fabricated and tested a PMN-PT based single cantilever (Fig. 1(a)) and an L-shape manipulator with IDEs (Fig. 1(c)) using the SDSU and UCI micro-fabrication facilities. Experimental results for the single cantilever and L-shape manipulator are shown in Fig. 5.

Fig. 5(a) shows the tip displacement response of a single cantilever beam with a tip proof mass under a step excitation (magnitude of $24\,\mu$m) at the base. Fig. 5(b) shows the frequency response of the L-shape structure. We carry out numerical computations for the natural frequencies and mode shapes for the L-shape structure using a finite element analysis (FEA) method. We list the comparison results in Table I for the first three natural frequencies.

For the L-shape manipulator, we use the same geometry cantilever beams. No proof mass has been mounted on the tip. Therefore, we have

$$M_t = 0, \quad L = 1, \quad M = 1, \quad \lambda_{w1} = \lambda_{w2} =: \lambda$$

and the natural frequency by (26) becomes

$$-3 - 8\cos(\lambda)\cosh\lambda - \cos(2\lambda) - \cosh(2\lambda) -$$
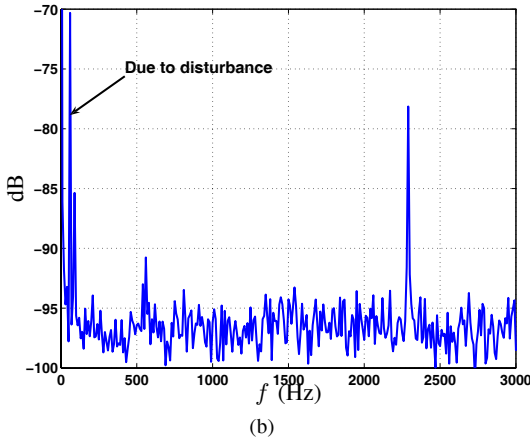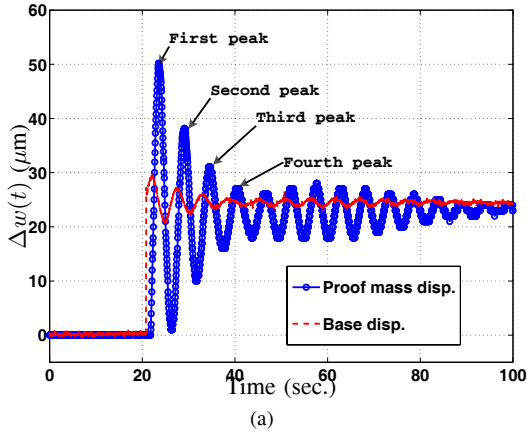$$3\cosh(2\lambda)\cos(2\lambda) = 0. \tag{28}$$

Fig. 5. (a) The tip displacement of a cantilever beam/mass system under a step input at the base. (b) Frequency response (magnitude) plot for the L-shape manipulator prototype.

TABLE I

COMPARISONS OF FIRST THREE NATURAL FREQUENCIES (IN HZ)

Modes	1st	2nd	3rd
Analytical	191	665	2155
FEA	195	636	2136
Experiments	210	560	2290

Solving the above equation numerically gives

$$\lambda_1 = 1.2165, \quad \lambda_2 = 2.2686, \quad \lambda_3 = 4.0832, \cdots.$$

The natural frequencies (in Hz) given by the flexural motion are then

$$\omega_i = \frac{1}{2\pi} \left(\frac{\lambda_i}{l}\right)^2 \sqrt{\frac{EI}{m}}, \quad i = 1, 2, \cdots,$$

where $l := l_1 = l_2$, $E := E_1 = E_2$, and $m := m_1 = m_2$. For the prototype shown in Fig. 2(b), $l = 12$ mm, $b = 1.5$ mm, $h = 120$ μm, $E = 105$ GPa, $\rho = 7900$ kg/m^3. The first three natural frequencies are then

$$\omega_1 = 191 \text{ Hz}, \quad \omega_2 = 665 \text{ Hz}, \quad \omega_3 = 2155 \text{ Hz}.$$

For the L-shape structure, the analysis matches very well with the FEA results. We find that the natural frequencies of the first three modes (in Table I) match our analysis

and FEA results. As shown in Fig. 5(b), we also observe a 60 Hz disturbance, which partially obscures the first mode in the experiments. We are currently investigating these experimental issues.

V. CONCLUSION

A modeling analysis of an L-shape manipulator using PMN-PT ferroelectric material and IDE electrodes is presented. The end effector of the L-shape design is capable of motion in multiple degrees of freedom (MDOF). The capability for MDOF motion is due to the IDE layout on the top and bottom surfaces of the structure as well as the properties of the PMN-PT material itself. We built a mathematical model to capture the dynamics between the input voltages and the deflections of the manipulator. We calculated and compared the natural frequencies of the manipulator prototype with FEA and experimental results, and found that they are consistent. The modeling scheme provides a mathematical foundation for manipulator control. Development and implementation of model-based manipulator control systems are currently ongoing research.

REFERENCES

[1] M. Sitti and H. Hashimoto, "Controlled Pushing of Nanoparticles: Modeling and Experiments," *IEEE/ASME Trans. Mechatron.*, vol. 5, no. 2, pp. 199–211, 2000.

[2] M. Sitti, "Atomic Force Microscope Probe Based Controlled Pushing for Nanotribological Characterization," *IEEE/ASME Trans. Mechatron.*, vol. 9, no. 2, pp. 343–349, 2004.

[3] G. Li, N. Xi, H. Chen, C. Pomeroy, and M. Prokos, ""Videolized" Atomic Force Microscopy for Interactive Nanomanipulation and Nanoassembly," *IEEE Trans. Nanotechnol.*, vol. 4, no. 5, pp. 605–615, 2005.

[4] J. Zhang, N. Xi, G. Li, H. Chan, and U. Wejinya, "Adaptable End Effector for Atomic Force Microscopy Based Nanomanipulation," *IEEE Trans. Nanotechnol.*, vol. 5, no. 6, pp. 628–642, 2006.

[5] T. Fukuda, F. Arai, and L. Dong, "Assembly of Nanodevices with Carbon Nanotubes Through Nanorobotic Manipulations," *Proc. IEEE*, vol. 91, no. 11, pp. 1803–1818, 2003.

[6] N. Xi and W. Li, "Recent Development in Nanoscale Manipulation and Assembly," *IEEE Trans. Automat. Sci. Eng.*, vol. 3, no. 3, pp. 194–198, 2006.

[7] S. Park and T. Shrout, "Ultrahigh Strain and Piezoelectric Behavior in Relaxor Based Ferroelectric Single Crystals," *J. Appl. Phys.*, vol. 82, pp. 1804–1811, 1997.

[8] Y. Hong, H. Park, S. Lee, K. Moon, and M. Levy, "Design of a Self-Sensing, Self-Actuating Piezoelectric Monomorph with Interdigitated Electrodes," in *Proc. SPIE*, vol. 5602, Philadelphia, PA, 2004, pp. 210–217.

[9] R. Vange, M. Levy, K. Moon, and Y. Hong, "Single Crystal Relaxor Ferroelectric Piezoactuator With Interdigitated Electrodes," *IEEE Trans. Ultrason., Ferroelect., Freq. Contr.*, vol. 51, no. 12, pp. 1593–1599, 2004.

[10] Y. Hong and K. Moon, "Interdigitated Single Crystal Piezoelectric Actuator," in *Proc. SPIE*, vol. 6048, 2005.

[11] K. Moon, J. Yi, Y. Hong, and A. Mathers, "Design of a PMN-PT-based Monolithic Nanomanipulator," in *Proc. SPIE Int. Sym. Optomech. Tech. (ISOT)*, Lausanne, Switzerland, 2007.

[12] M. Gürgöze, "On the Dynamic Analysis of a Flexible L-Shape Structure," *J. Sound Vib.*, vol. 211, no. 4, pp. 683–688, 1998.

[13] D. Oguamanam, J. Hansen, and G. Heppler, "Vibration of Arbitrarily Oreiented Two-Member Open Frames with Tip Mass," *J. Sound Vib.*, vol. 209, no. 4, pp. 651–669, 1998.

[14] G. Heppler, D. Oguamanam, and J. Hansen, "Vibration of a Two-Member Open Frame," *J. Sound Vib.*, vol. 263, no. 2, pp. 299–317, 2003.

[15] L. Meirovitch, *Principles and Techniques of Vibrations.* Upper Saddle River, NJ: Prentice Hall, 1997.